



RESEARCH ARTICLE

10.1002/2015JD024039

Stratospheric temperature changes during the satellite era

Dian J. Seidel¹, Jian Li^{2,3}, Carl Mears⁴, Isaac Moradi⁵, John Nash^{6,7}, William J. Randel⁸, Roger Saunders⁶, David W. J. Thompson⁹, and Cheng-Zhi Zou³

Key Points:

- Discrepancies remain among stratospheric temperature climate data records
- Data for 1979–2013 reveal distinct solar, ENSO, aerosol, QBO, and trend signals
- Piecewise-linear trends indicate cooling before 1995 and no trend thereafter

Correspondence to:

D. J. Seidel,
dian.seidel@noaa.gov

Citation:

Seidel, D. J., J. Li, C. Mears, I. Moradi, J. Nash, W. J. Randel, R. Saunders, D. W. J. Thompson, and C.-Z. Zou (2016), Stratospheric temperature changes during the satellite era, *J. Geophys. Res. Atmos.*, 121, 664–681, doi:10.1002/2015JD024039.

Received 3 AUG 2015

Accepted 21 DEC 2015

Accepted article online 23 DEC 2015

Published online 20 JAN 2016

¹NOAA Air Resources Laboratory, College Park, Maryland, USA, ²Earth Resources Technology, Inc., Laurel, Maryland, USA, ³NOAA Center for Satellite Applications and Research, College Park, Maryland, USA, ⁴Remote Sensing Systems, Santa Rosa, California, USA, ⁵Cooperative Institute for Climate and Satellites, University of Maryland, College Park, Maryland, USA, ⁶Meteorological Office, Exeter, UK, ⁷Retired, ⁸National Center for Atmospheric Research, Boulder, Colorado, USA, ⁹Department of Atmospheric Science, Colorado State University, Fort Collins, Colorado, USA

Abstract Satellite-based layer average stratospheric temperature (T) climate data records (CDRs) now span more than three decades and so can elucidate climate variability associated with processes on multiple time scales. We intercompare and analyze available published T CDRs covering at least two decades, with a focus on Stratospheric Sounding Unit (SSU) and Microwave Sounding Unit (MSU) CDRs. Recent research has reduced but not eliminated discrepancies between SSU CDRs developed by NOAA and the UK Meteorological Office. The MSU CDRs from NOAA and Remote Sensing Systems are in closer agreement than the CDR from the University of Alabama in Huntsville. The latter has a previously unreported inhomogeneity in 2005, revealed by an abrupt increase in the magnitude and spatial variability of T anomaly differences between CDRs. Although time-varying biases remain in both SSU and MSU CDRs, multiple linear regression analyses reveal consistent solar, El Niño–Southern Oscillation (ENSO), quasi-biennial oscillation, aerosol, and piecewise-linear trend signals. Together, these predictors explain 80 to 90% of the variance in the near-global-average T CDRs. The most important predictor variables (in terms of percent explained variance in near-global-average T) for lower stratospheric T measured by MSU are aerosols, solar variability, and ENSO. Trends explain the largest percentage of variance in observations from all three SSU channels. In MSU and SSU CDRs, piecewise-linear trends, with a 1995 break point, indicate cooling during 1979–1994 but no trend during 1995–2013 for MSU and during 1995–2005 for SSU. These observational findings provide a basis for evaluating climate model simulations of stratospheric temperature during the past 35 years.

1. Introduction

Under the auspices of the World Climate Research Programme/Stratosphere-troposphere Processes and their Role in Climate (SPARC) Temperature Trends Activity, multiple studies have comprehensively analyzed stratospheric temperature variability and trends from both observational and modeling perspectives [Ramaswamy *et al.*, 2001; Shine *et al.*, 2003; Randel *et al.*, 2009b; Seidel *et al.*, 2011; Thompson *et al.*, 2012]. Over time, the observational emphasis of these investigations has shifted from ground-based and in situ observing systems (rocketsondes, radiosondes, and lidar) with limited station networks toward satellite-based systems.

The most recent of these SPARC investigations [Thompson *et al.*, 2012] focused on comparison of layer average stratospheric temperature (T) observations for 1979–2005 from the satellite-borne Stratospheric Sounding Unit (SSU) and reported strikingly different T trends from two data sets derived from those observations. Thompson *et al.* [2012] also noted discrepancies among three data sets derived from Microwave Sounding Unit (MSU) and Advanced MSU (AMSU) observations and between the various satellite observations and a suite of simulations by both chemistry-climate models and atmosphere-ocean global climate models.

Reanalysis-based stratospheric temperature data products have not been a major focus of the SPARC Temperature Trends Activity, mainly because of concerns that they contain time-varying biases and so are not reliable indicators of long-term trends [Thorne and Vose, 2010; Dee *et al.*, 2010]. Recent efforts to improve reanalyses have focused on this concern, and the current generation of reanalyses may more reliably reflect real stratospheric temperature changes [Simmons *et al.*, 2014; Kobayashi *et al.*, 2015]. A separate SPARC activity, the SPARC Reanalysis Intercomparison Project, is comprehensively evaluating current reanalysis data products, including stratospheric temperature [Errera *et al.*, 2015].

©2015. The Authors.

This is an open access article under the terms of the Creative Commons Attribution-NonCommercial-NoDerivs License, which permits use and distribution in any medium, provided the original work is properly cited, the use is non-commercial and no modifications or adaptations are made.

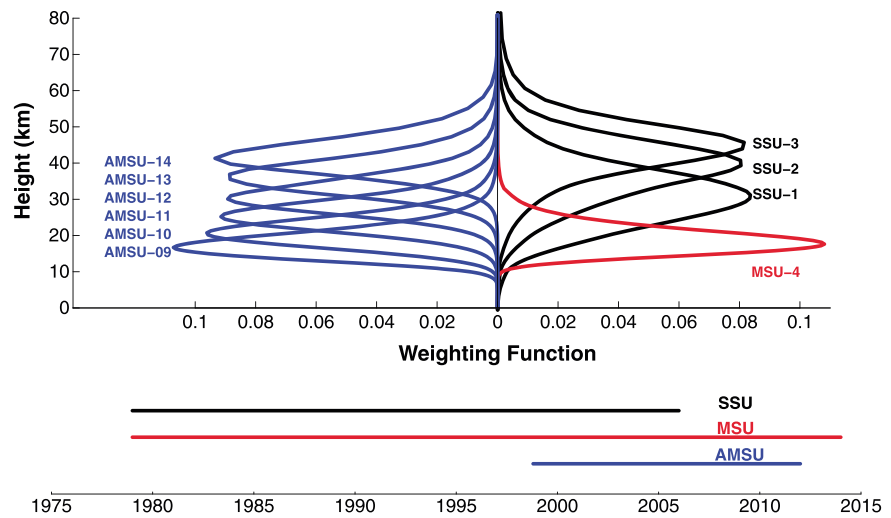


Figure 1. (top) Vertical weighting function and (bottom) time period of data availability of the stratospheric temperature climate data records, from different instruments and different channels, used in this study.

In this contribution, we focus exclusively on satellite observations of stratospheric T , delve further into data set comparisons, and investigate various signals of T variability, including trends. Several factors motivate this focus. First, satellite observations of the stratosphere started about a half century ago, and near-continuous, multidecadal records from series of similar instruments starting in 1979 now provide records spanning 35 years and covering several time scales of stratospheric variability. Moreover, the last two decades have seen no major volcanic eruptions influencing stratospheric aerosol loading and associated T response, which may allow other climate signals to emerge more clearly than prior to 1995. Second, the long sought, and often found, stratospheric cooling in the presatellite era and in the first two decades of the satellite era appears to have decelerated or ceased [Long and Christy, 2014]. In the lower stratosphere, where T responds to changes in stratospheric ozone, this deceleration has been associated with slowly decreasing stratospheric concentrations of ozone-depleting substances and gradual ozone layer recovery [Thompson and Solomon, 2009; Ferraro et al., 2015]. But little work has specifically focused on this period or on T changes in the middle and upper stratosphere. Third, motivated both to resolve the “mystery of recent stratospheric temperature trends” identified by Thompson et al. [2012] and to provide better documentation of their data set construction methods, both SSU research teams have developed new versions of their data sets [Zou et al., 2014; Nash and Saunders, 2015], which warrant reexamination of the issue.

The two specific goals of this study are (1) to update the studies mentioned above by reviewing the current state of satellite-based stratospheric T climate data records (CDRs) and comparing existing CDRs based on the same raw measurements and (2) to provide new insights into the space-time structure of, and possible explanations for, stratospheric T variability. Previous studies [e.g., Naujokat, 1981; Calvo Fernandez et al., 2004; Seidel et al., 2004; Hood et al., 2010; Gillett et al., 2011; Forbes et al., 2014; Mitchell et al., 2014, and references therein] have addressed the latter problem but less comprehensively and systematically, using fewer and shorter CDRs, using globally or zonally averaged rather than gridded data, focusing on the lower stratosphere only, and examining only some of the potential explanations for variability.

2. Data and Methods

2.1. Stratospheric Temperature Climate Data Records

We analyze CDRs of stratospheric T from satellite platforms for the period 1979–2013 that are documented in the peer-reviewed literature and that offer continuous, near-global sampling of the stratosphere for at least two decades. We do not attempt to construct new CDRs by merging data from existing CDRs, because this is a complex undertaking, beyond the scope of this paper.

The CDRs include three lower stratospheric records based on MSU Channel 4 (MSU-4) observations merged with AMSU observations; two new sets of CDRs based on SSU Channels 1, 2, and 3 (SSU-1, SSU-2, and SSU-3) [Zou et al., 2014; Nash and Saunders, 2015]; and one set of CDRs for AMSU Channels 9–14 [Wang and Zou,

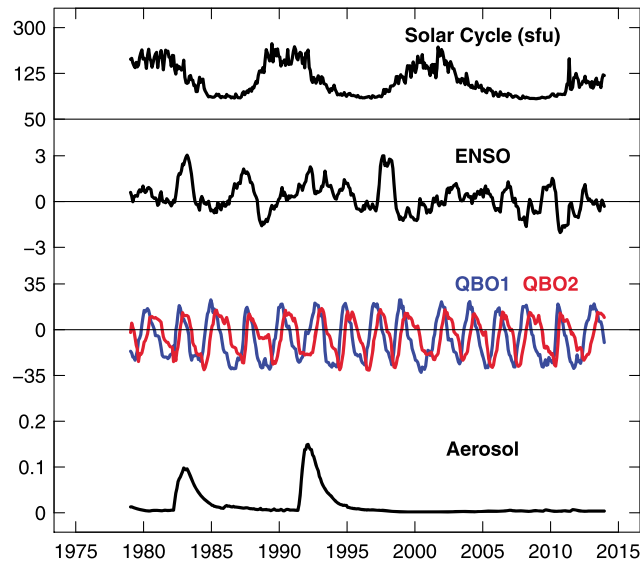


Figure 2. Predictor time series used in multiple regression analyses for 1979–2013. Units for the solar cycle predictor are solar flux units ($1 \text{ sfu} = 10^{-22} \text{ W m}^{-2} \text{ Hz}^{-1}$). The ENSO and QBO indices and stratospheric aerosol optical depth are dimensionless.

produced by *Zou et al.* [2006], *Mears and Wentz* [2009], and *Christy et al.* [2003], respectively. Most of the UAH MSU-4 data used here is version 5.6, the version of record during the course of this study, documented by *Christy et al.* [2003], but one analysis employs a “beta” version 6.0 of UAH MSU-4 data, released in April 2015.

For SSU CDRs, we refer to the *Zou et al.* [2014] CDR as NOAA and the *Nash and Saunders* [2015] CDRs as UKMO (UK Meteorological Office). We use only the most recent versions of all CDRs, but note that the UKMO SSU CDRs [*Nash and Saunders*, 2015] are global averages, at 6 month resolution, whereas the prior version [*Randel et al.*, 2009b] had 10° latitude and 1 month resolution.

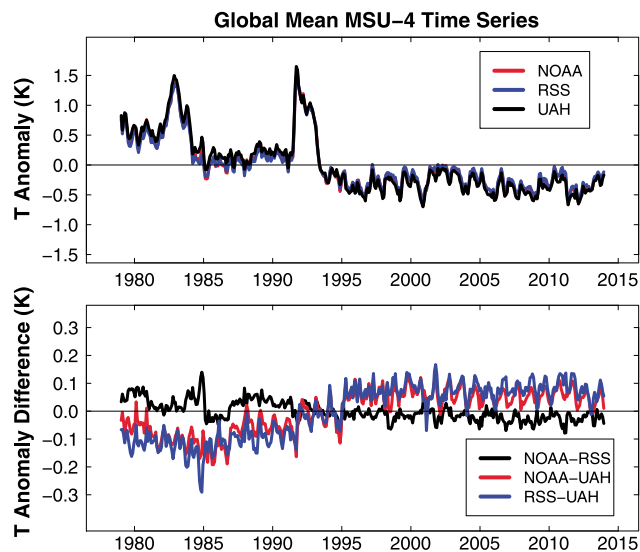


Figure 3. (top) Near-global-average (84°S – 84°N) monthly temperature anomaly time series from three climate data records derived from Microwave Sounding Unit Channel 4 observations for 1979–2013. (bottom) Paired difference times series based on the anomaly time series.

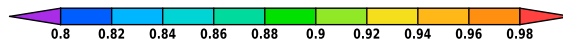
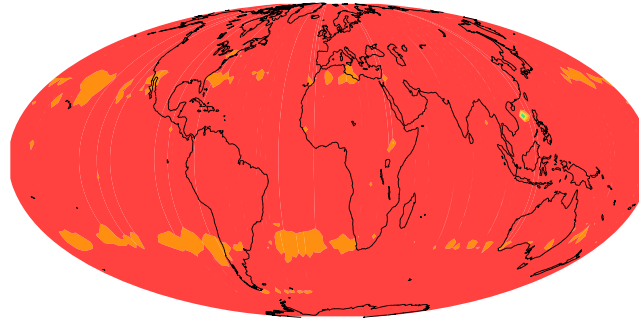
2014]. Of these, only the merged MSU/AMSU CDRs cover the full period 1979–2013; SSU CDRs end in 2005, and AMSU CDRs begin in 1999. Although AMSU observations continue to the present, data since 2011 have not yet been incorporated in a CDR. (We have a separate effort to do so underway.) A schematic representation of the time span and vertical layers sampled by each of these CDRs is shown in Figure 1. Because the AMSU record is short, most of our analysis addresses the MSU-4 and SSU CDRs.

We use the abbreviation MSU-4 to denote the merged MSU/AMSU record and the following abbreviations to distinguish the MSU-4 CDRs: NOAA (National Oceanic and Atmospheric Administration), RSS (Remote Sensing Systems), and UAH (University of Alabama in Huntsville) for CDRs produced by *Zou et al.* [2006], *Mears and Wentz* [2009], and *Christy et al.* [2003], respectively.

An obvious inference from Figure 1 is the lack of CDRs covering the middle and upper stratosphere for the full satellite era. *McLandress et al.* [2015] recently merged SSU and AMSU data using Michelson Interferometer for Passive Atmospheric Sounding measurements to link the two, restricting their analysis to monthly, near-global-average time series. Some authors of this paper are engaged in other efforts to merge SSU and AMSU data and to merge SSU data with other stratospheric *T* observations (*W. J. Randel et al.*, Stratospheric temperature trends over 1979–2015 derived from combined SSU, MLS and SABER satellite 617 observations, submitted to *Journal of Climate*, 2015), to fill this significant gap.

Monthly *T* anomaly time series were computed using gridded monthly *T* data. The mean annual cycle for the full period of record was removed by subtracting the long-term monthly mean

Correlation between NOAA and RSS



Correlation between UAH and RSS

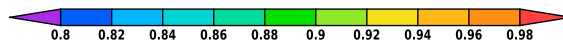
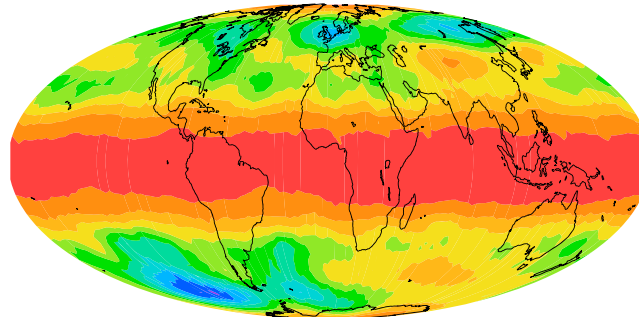


Figure 4. Maps of linear correlation coefficients for MSU-4 temperature anomaly time series for (top) NOAA and RSS and (bottom) UAH and RSS climate data records.

from each monthly mean value, for each calendar month, at each grid point. This procedure for creating anomalies was not applied to UKMO SSU data, which are not available at gridded or zonal-mean resolution and which are provided as global T anomalies at 6 month resolution.

The CDRs are all publicly available, as follows: MSU-4 from RSS (<http://www.remss.com/measurements/upper-air-temperature/>); MSU-4 version 5.6 from UAH (<http://vortex.nsstc.uah.edu/data/msu/t4/>); MSU-4 beta version 6.0 (<http://www.nsstc.uah.edu/data/msu/v6.0beta/tls/>); MSU-4, SSU, and AMSU from NOAA (<http://www.star.nesdis.noaa.gov/smcd/emb/mecat/products.php>); and SSU from UKMO (ftp://ftp.star.nesdis.noaa.gov/pub/smcd/emb/mecat/data/SSU/SSU_UKMO_V2/).

2.2. Multiple Regression Analysis and Predictor Time Series

Global-mean and zonal-mean (at 2.5° latitude resolution) stratospheric T variations are analyzed using multiple linear regression analysis. Predictor variables, all previously shown to be associated with stratospheric T change, include the following:

1. A solar activity index, specifically 10.7 cm radio flux at Ottawa/Penticton [*Tapping and Morton, 2013*], available at http://www.ngdc.noaa.gov/stp/space-weather/solar-data/solar-features/solar-radio/noontime-flux/penticton/penticton_adjusted/tables/table_drao_noontime-flux-adjusted_monthly.txt.

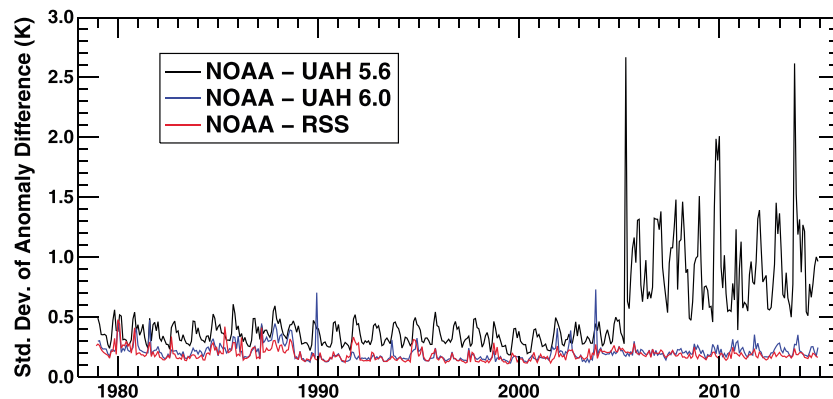


Figure 5. Time series of spatial standard deviations of differences in monthly MSU-4 temperature anomalies between paired MSU-4 climate data records. For each month, gridded T anomalies at 2.5° latitude/longitude resolution are subtracted from gridded T anomalies based on the NOAA CDR, and the standard deviation of the gridded differences is computed using area weighting. In addition to the RSS and UAH (version 5.6) MSU-4 CDRs, this figure also compares UAH version 6.0 (beta release version).

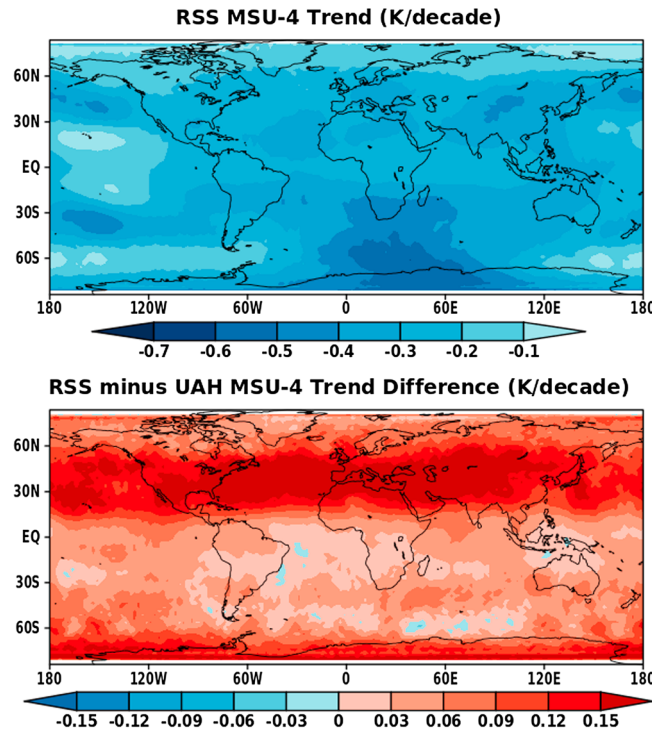


Figure 6. (top) Map of linear trends (K/decade) for 1979–2013 in RSS MSU-4 T anomaly time series. (bottom) Map of differences in T trends from RSS and UAH data.

2. An El Niño–Southern Oscillation (ENSO) index, specifically the Multivariate ENSO Index [Wolter and Timlin, 2011], available at <http://www.esrl.noaa.gov/psd/enso/mei/table.html>.
3. An index of the quasi-biennial oscillation (QBO), based on zonal winds over Singapore [Naujokat, 1986], available at <http://www.geo.fu-berlin.de/en/met/ag/strat/produkte/qbo/index.html>. Following Wallace et al. [1993], we derive two orthogonal basis functions from the wind profile data to capture the downward propagation of the QBO signal over several months [Randel et al., 1999].
4. An index of stratospheric aerosol optical depth [Sato et al., 1993], available at <http://data.giss.nasa.gov/modelforce/strataer/>. This index was available only through September 2012, and we extrapolated the low 2012 values through 2013, based on current understanding of recent stratospheric aerosol concentrations (J.-P. Vernier, NASA, personal communication, 2014).

5. Time, a piecewise-linear term to represent two monotonic, nonaccelerating trends. The slopes of the two segments are obtained from the regression. The breakpoint is fixed at January 1995, as explained in section 3.2.1 below.

With the exception of the time terms, each of the predictors is an imperfect representation of a complex physical phenomenon influencing stratospheric temperature. The multiple regression results are likely to be sensitive to uncertainty in these representations. Although we recognize this source of uncertainty, we have not attempted to quantify it. That would require estimates both of uncertainties in individual indices (which are not generally available) and of the spread among different indices of the same phenomena (e.g., the differences between the total solar irradiance and 10.7 cm radio flux indices of solar variability, and the spread of the many ENSO indices in the literature).

However, we do report uncertainty estimates for regression coefficients using 95% confidence intervals, based on the regression fits and taking into account time series autocorrelation by adjusting the degrees of freedom. Figure 2 illustrates the predictor time series. All are dimensionless variables, except for the solar index, with solar flux units (where $1 \text{ sfu} = 10^{-22} \text{ W m}^{-2} \text{ Hz}^{-1}$). Except for trend terms, predictor time series were normalized by their respective standard deviations. Resulting trends are expressed in K per decade, and regression coefficients are expressed in K per standard deviation.

3. Results

This section focuses first on quantitative and qualitative intercomparison of CDRs, with particular attention to the multidecadal SSU and MSU CDRs. For completeness, the shorter AMSU CDRs are also presented because they provide some information on recent T changes in the middle and upper stratosphere and because they are likely to be merged with the SSU records in the future. Then we use the MSU and SSU CDRs to elucidate aspects of the observed T variability.

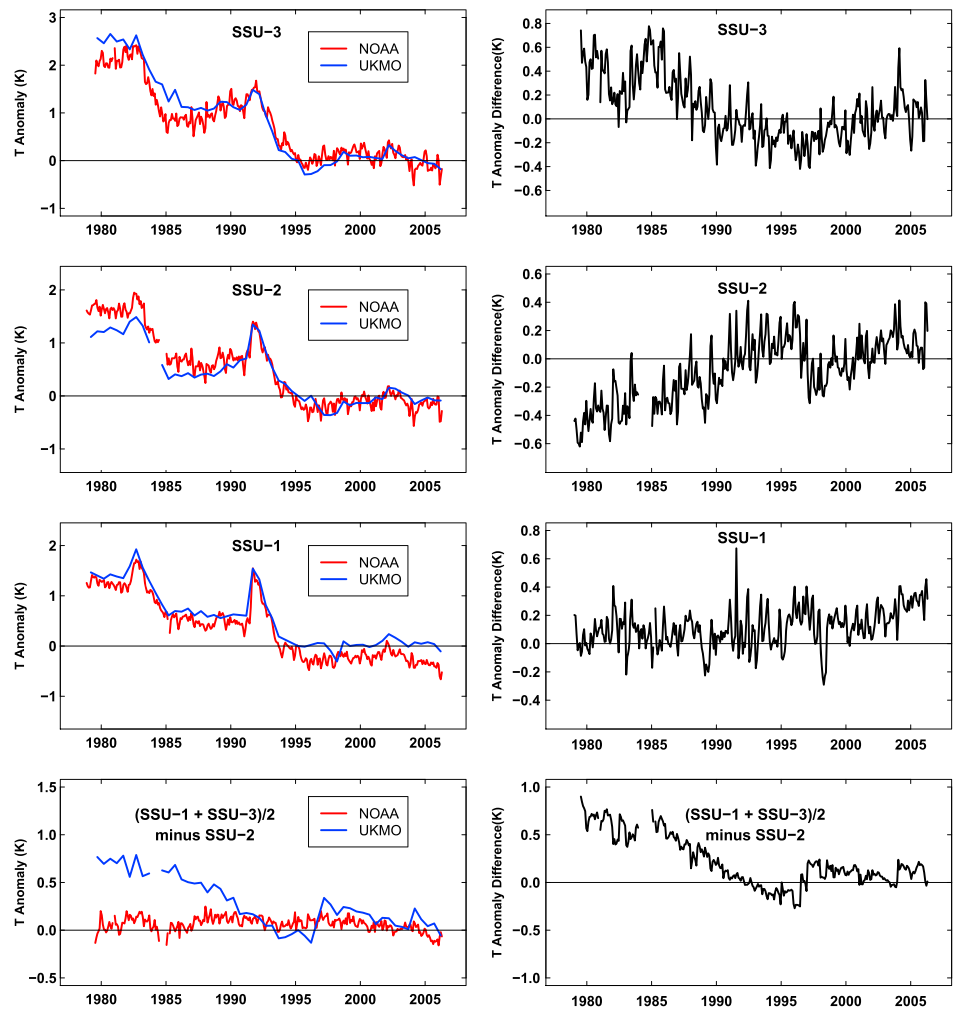


Figure 7. (left column) Near-global-average (84°S – 84°N) temperature anomaly time series from two climate data records derived from Stratospheric Sounding Unit observations for 1979–2005, for SSU-1, SSU-2, and SSU-3, and for the difference between the average of SSU-1 and SSU-3 anomalies and SSU-2 anomalies. NOAA and UKMO data are shown at monthly and 6 monthly resolution, respectively. (right column) Anomaly difference time series (UKMO minus NOAA) for SSU-1, SSU-2, and SSU-3, and for the difference between the average of SSU-1 and SSU-3 anomalies and SSU-2 anomalies.

3.1. Intercomparison of Climate Data Records

3.1.1. Intercomparison of Microwave Sounding Unit Climate Data Records

Figure 3 shows near-global-average lower stratospheric T anomaly time series from the three MSU-4 CDRs, as well as paired difference time series. All three CDRs reveal T ranges of ~ 2 K over the 35 year record, with higher and more variable T before 1995 than after. The difference time series show NOAA and RSS CDRs to be within ~ 0.15 K of each other, with a long-term relative drift indicating greater cooling in the NOAA CDR than in the RSS CDR. The UAH CDR indicates a larger time-varying bias with respect to both the NOAA and RSS records, with UAH showing $T \sim 0.1$ K higher during 1979–1995 and ~ 0.1 K lower thereafter. Thus, the near-global-average long-term cooling during 1979–2013 is greater in the UAH record than in the other two.

While these differences among the MSU-4 CDRs are small compared with the variability in stratospheric T that they all reveal, the differences are nontrivial compared with estimated stratospheric T trends. For example, Thompson *et al.* [2012] report 1979–2005 trends of ~ 0.4 K/decade in MSU-4 CDRs, so the long-term drift of about 0.2 K over 1979–2013 between UAH and the other two CDRs is $\sim 15\%$ of the estimated trend. The drift is also comparable to the Monte Carlo estimated 2 sigma uncertainty in MSU-4 temperature changes [Mears *et al.*, 2011].

But the differences between UAH and the other two data sets are not fully explained by near-global-average long-term trends; they also have spatial structure and shorter-term manifestations. Examination of the gridded

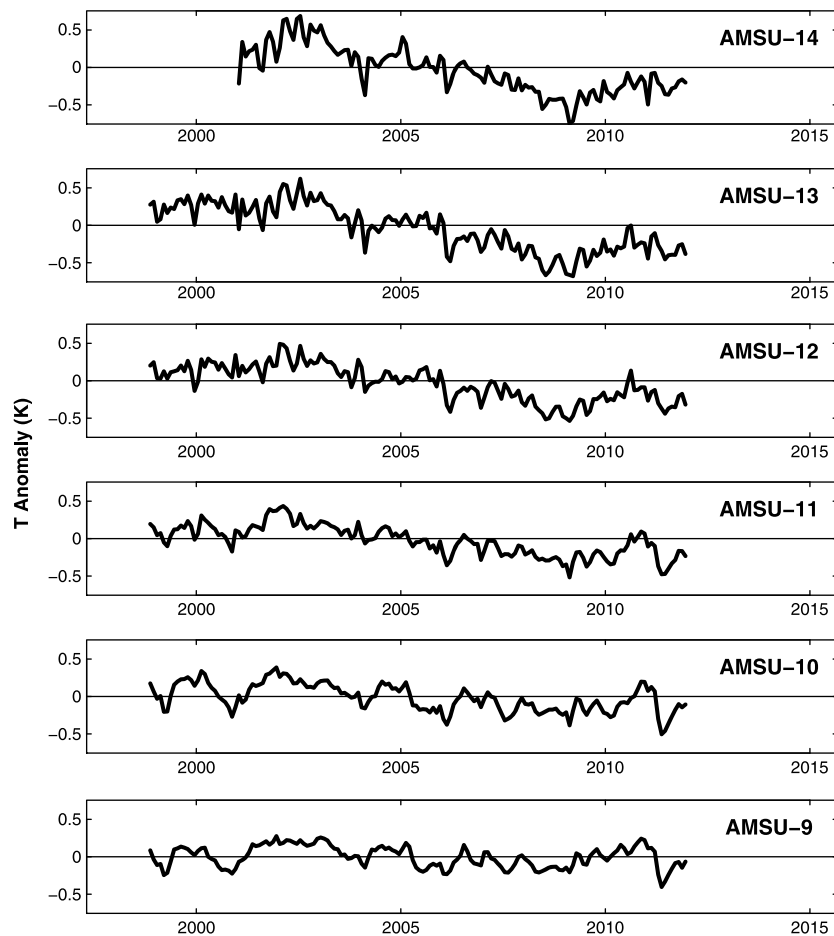


Figure 8. Near-global-average (84°S – 84°N) monthly temperature anomaly time series derived from Channels 9–14 of the Advanced Microwave Sounding Unit for 1999–2011.

anomaly time series shows regional patterns in their degree of association. Linear correlations between the NOAA and RSS time series exceed 0.95 at virtually all grid boxes (Figure 4, top). Correlations between RSS and UAH (Figure 4, bottom) and between NOAA and UAH (not shown but very similar to Figure 4, bottom) are similarly high within 20° latitude of the equator but are lower (as low as 0.8) at higher latitudes.

The differences in high-latitude T variability seen in Figure 4 arise from both short- and long-term structures. There is a distinct annual periodicity in the time series of differences (Figure 3), and zonal-mean anomaly time series differences (not shown) reveal this pattern to be exaggerated in high-latitude regions of both hemispheres. Surprisingly, after 2005 UAH data show larger anomalies than the other CDRs, particularly in February and March in the Northern Hemisphere and in October, November, and December in the Southern Hemisphere.

The time series in Figure 5 reveal this inhomogeneity in version 5.6 of UAH MSU-4 data. As background, we note that versions 5.1 through 5.6 have been the versions of record since 2002 [Christy *et al.*, 2003], and version 6.0 was released as a “beta” version during the final stages of this research. Figure 5 compares the NOAA MSU-4 CDR with the RSS, UAH version 5.6, and UAH beta version 6.0 data. For each month, we subtracted gridded T anomalies at 2.5° latitude/longitude resolution from gridded T anomalies based on the NOAA CDR, and the standard deviation of the gridded differences was computed using area weighting. Figure 5 shows that the spatial differences between NOAA and RSS data have standard deviations of ~ 0.2 K (red curve). The differences between NOAA and UAH version 5.6 are ~ 0.4 K before 2005 and ~ 1.0 K thereafter, with a distinct annual periodicity, while the differences between NOAA and UAH version 6.0 are much smaller, comparable to those between NOAA and RSS and to those between RSS and UAH version 6.0.

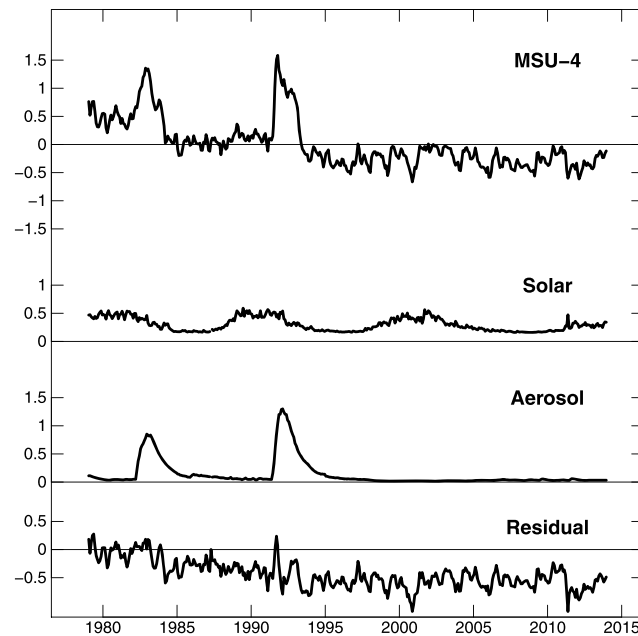


Figure 9. Time series of monthly T anomalies from (first panel from the top) the RSS MSU-4 climate data record (same as in Figure 3), fits to (second panel) solar cycle and (third panel) aerosol predictors, and (fourth panel) residuals.

MSU-4 CDRs, and Figure 6 shows the spatial structure of this difference by comparing simple linear trends in UAH and RSS CDRs. (Comparison of UAH and NOAA CDRs are similar.) The RSS CDR indicates long-term (1979–2013) cooling at all locations, from ~ 0.1 to 0.6 K/decade, with greatest cooling in Southern Hemisphere high latitudes (Figure 6, top). The UAH CDR shows greater cooling, with the largest differences (>0.1 K/decade) in Northern Hemisphere midlatitudes (Figure 6, bottom), where the RSS trend is ~ 0.25 K/decade.

In summary, we find that (1) there remain discrepancies among the three MSU-4 CDRs; (2) the NOAA and RSS CDRs are in better agreement with each other than with UAH version 5.6; (3) the UAH version 5 CDR has much higher spatial variability after 2005 than before; (4) a UAH “beta” version 6 does not exhibit this artifact; and (5) the artifact influences the magnitude and spatial pattern of multidecadal trends.

3.1.2. Intercomparison of Stratospheric Sounding Unit Climate Data Records

Near-global-average T anomaly time series for the three SSU channels, for the NOAA and UKMO CDRs (Figure 7, left column), show grossly similar T changes as in the MSU-4 records. Temperatures are higher before 1995 than after. Differences between the UKMO and NOAA CDRs (Figure 7, right column) are as large as ± 0.5 K in all three SSU channels. All three channels, but especially SSU-2 and SSU-3, exhibit long-term drifts between the two CDRs, with NOAA showing more cooling than UKMO for SSU-1 and SSU-2, and UKMO showing more cooling than NOAA for SSU-3. Because the UKMO CDR is a global-mean record, we cannot determine if a regional pattern exists in the differences between the UKMO and NOAA records.

Although these differences are smaller than those found in the earlier versions of the CDRs examined by Thompson *et al.* [2012], and although structural uncertainty can be expected due to different approaches to CDR construction [Thorne *et al.*, 2005], the magnitude of the differences between the new versions remains larger than the uncertainty estimates given by both research teams, despite concerted efforts to understand and reconcile them. The differences between the two sets of SSU CDRs are larger than the differences among the three MSU-4 CDRs discussed above, as was the case for the earlier versions [Thompson *et al.*, 2012].

To evaluate the vertical consistency of SSU CDRs, Figure 7 (bottom panels) show the differences between the average of SSU-1 and SSU-3 anomalies and SSU-2 anomalies, from both UKMO and NOAA records (left) and their difference (right). Seidel *et al.* [2011, Figure 7] suggested that this difference should be close to 0, as was the case in model simulations. An earlier version of UKMO SSU data [Randel *et al.*, 2009b] showed very large

This previously unreported time-varying bias in UAH version 5.6 data is also present in UAH versions 5.3 and 5.4. Version 5.1 ends in 2003, and versions 5.2 and 5.5 do not include MSU-4 data. Thus, results of studies based on UAH MSU-4 data since 2005 could have been influenced by this artifact. The remainder of this paper uses version 5.6, but we have repeated all our analyses using version 6.0 and find little sensitivity to this choice in the multiple regression results to follow. This does not guarantee that other studies, focusing on other aspects of the data set, would also be insensitive to the choice. Indeed, versions of Figures 3 and 4 involving UAH MSU-4 version 6.0 (not shown) indicates better agreement among the three near-global-average time series, without the annual periodicity in difference time series involving UAH data (Figure 3).

Figure 3 suggests greater cooling in UAH than in RSS or NOAA near-global-average

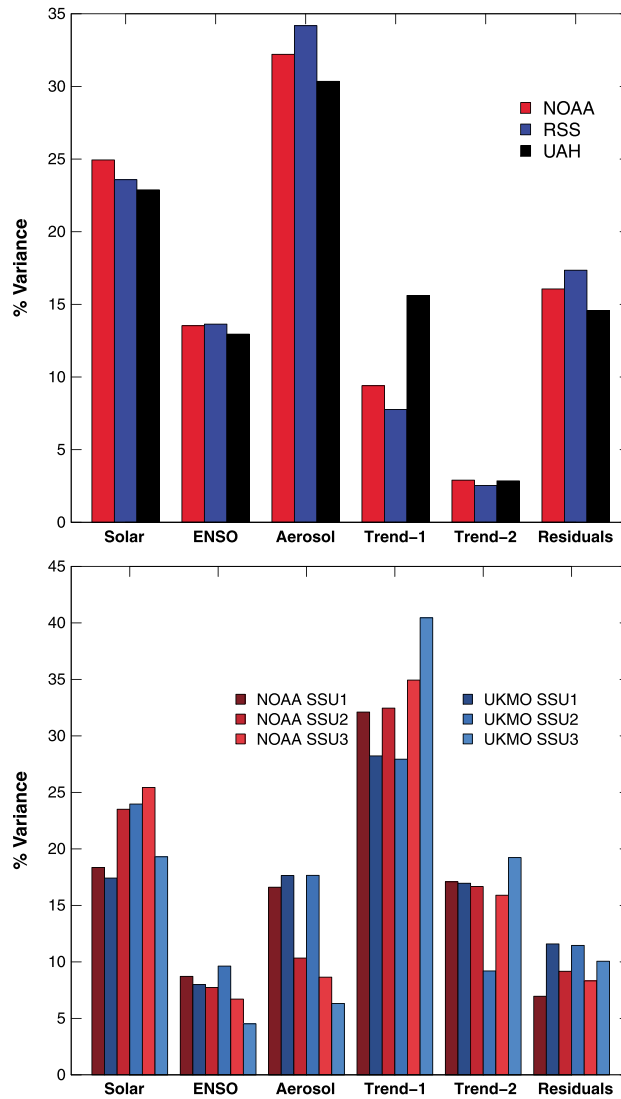


Figure 10. Percent of variance in near-global-average temperature anomaly time series explained by predictors. (top) Results from three MSU-4 climate data records for 1979–2013. (bottom) Results for two climate data records, for all three SSU channels. The QBO predictors are not included because they explain less than 1% of the total variance in all of the near-global-average temperature climate data records. Trend-1 refers to the 1970–1994 time period, and Trend-2 refers to the period beginning January 1995 and ending in 2013 and 2005 for MSU-4 and SSU, respectively.

consistent with MSU-4 results discussed above. Although the record is short, these net changes are qualitatively consistent with the expectation of middle and upper stratospheric cooling due to greenhouse gas increases and little *T* change in the lower stratosphere due to the lack of stratospheric ozone trend. We do not explore the AMSU records further here. Additional analysis will be warranted once they have been extended to the present. Both extended AMSU CDRs and CDRs merging SSU and AMSU observations are under development.

3.2. Multiple Regression Results

This section presents a multiple regression analysis of *T* anomalies using the predictor variables presented in section 2.2. We first provide motivation for treatment of *T* trends as a piecewise-linear function, and then we show regression results for MSU-4 and SSU CDRs.

differences that were deemed unrealistic [Seidel et al., 2011, Figure 7], while the current CDRs from NOAA exhibit much smaller differences [Zou et al., 2014, Figure 18]. Direct comparison in Figure 7 (bottom panels) shows differences within ± 0.2 K in the NOAA CDRs but as large as 0.8 K in the UKMO CDRs. The UKMO differences are smaller than those shown in Seidel et al. [2011]. Thus, both current NOAA and UKMO SSU CDRs exhibit greater vertical consistency than earlier versions, and the CDRs from NOAA are more consistent with models in terms of vertical structure than those from UKMO.

The two SSU CDRs were created using different data adjustment and merging methods, the validity of which influences both the reliability of the CDRs and their differences. Assimilation of the SSU radiances along with other satellite observations (e.g., from the High Resolution Infrared Sounder, MSU, and GPS radio occultation bending angles) in future reanalyses will provide new insights, as the intersatellite and diurnal biases are adjusted by the reanalysis data assimilation systems.

3.1.3. Advanced Microwave Sounding Unit Climate Data Records

Data from the six AMSU channels (Figure 8) show near-global-average *T* anomalies over 1999–2011. The stratospheric layer sampled by channels 11–14 (covering the region previously sampled by the three SSU channels, Figure 1) have experienced cooling over the 13 year period, particularly during 2003–2009. The lower stratospheric levels show less variability and little net change, con-

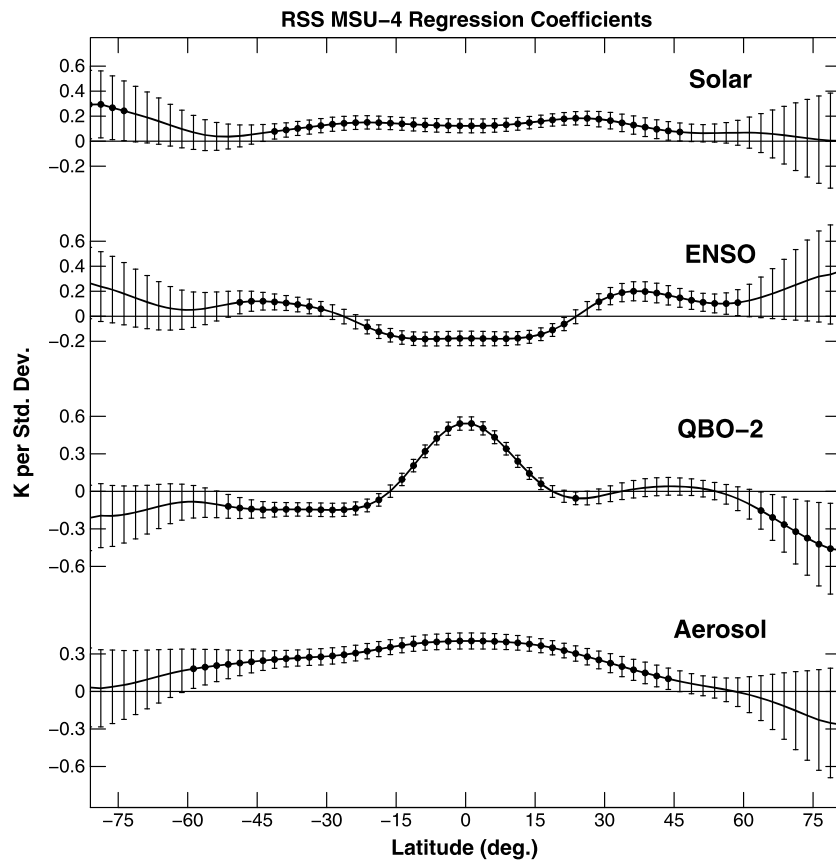


Figure 11. Regression coefficients (K per standard deviation) as a function of latitude, at 2.5° latitude resolution, and their 95% confidence intervals, obtained from multiple linear regression of zonal-mean MSU-4 temperature anomaly time series from the RSS MSU-4 climate data record. Coefficients are shown with filled circles at latitudes where the 95% confidence intervals do not encompass 0. Results for the UAH and NOAA records are very similar and are not shown.

3.2.1. Piecewise-Linear Trends

Greenhouse gas increases and stratospheric ozone decreases lead to stratospheric cooling, in contrast with expected surface warming. Confident detection and estimation of stratospheric T trends has long been a research goal, which the SPARC Temperature Trends Activity has sustained for more than 20 years. Methods for estimating trends have generally involved use of deseasonalized monthly T anomaly time series, and often [e.g., Thompson *et al.*, 2012; Long and Christy, 2014] the slope of a linear fit serves as a simple measure of trend (as in the discussion of MSU-4 CDRs in section 3.1.1 above). More complex multiple regression treatments involve accounting for other types of variations in the time series [e.g., Randel *et al.*, 2009b, and submitted, 2015] but still maintaining a single linear slope term as a trend estimate.

However, previous studies [Pawson *et al.*, 1998; Seidel and Lanzante, 2004; Ramaswamy *et al.*, 2006] have argued in favor of piecewise-linear functions to characterize stratospheric T changes. Insofar as trends are driven by greenhouse gas and ozone changes, the turnaround in stratospheric ozone depletion is a strong argument in favor of a piecewise-linear approach. Using this argument, Ferraro *et al.* [2015] describe a cessation of stratospheric cooling in the early 21st century.

As described in section 2.2, our multiple regression methodology involves two trend segments. Using the RSS MSU-4 CDR as an example, Figure 9 illustrates the motivation for this approach. Along with trends, solar and stratospheric aerosol variations could account for T variations on decadal time scales, whereas QBO and ENSO vary on interannual time scales. Figure 9 shows the T anomaly time series (first panel from the top), solar and aerosol regression fits (which together explain about half the total T anomaly variance), and the time series of residuals (fourth panel). The residuals have an obvious downward slope during 1979–1994 and a much smaller

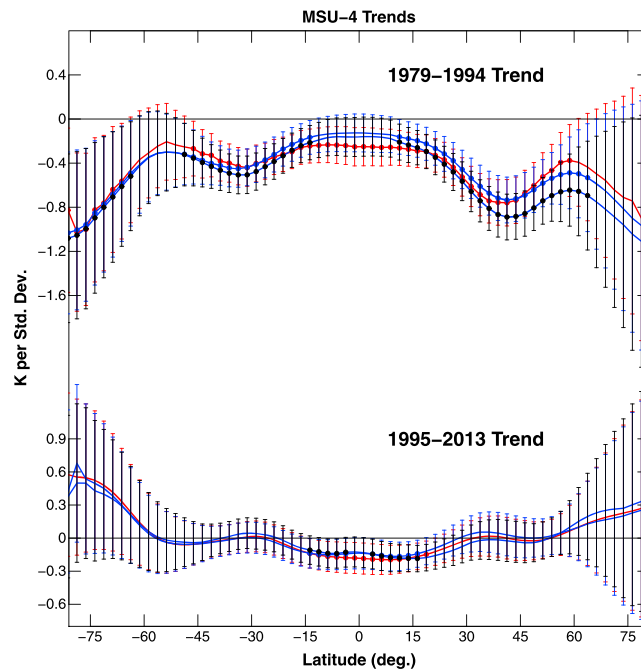


Figure 12. Trend estimates (K per decade) as a function of latitude, at 2.5° latitude resolution, obtained from multiple linear regression of zonal-mean MSU-4 temperature anomaly time series from NOAA, RSS, and UAH (red, blue, and black, respectively) climate data records. Estimates for (top) 1979–1994 and (bottom) 1995–2013 are shown as filled circles at latitudes where the 95% confidence intervals do not encompass 0.

are not shown in the plot. The six predictors together explain at least 83% of the variance during 1979–2013, and the regression coefficients (not shown) from the three CDRs agree within their 95% confidence intervals. Figure 11 shows regression coefficients as a function of latitude for selected predictors from the RSS CDR (results from the UAH and NOAA CDR are very similar), and Figure 12 shows trend estimates for all three CDRs. We proceed to discuss each term of the MSU-4 regressions based on near-global-average and zonal-average data.

Variability in stratospheric aerosol loading explains the largest fraction of MSU-4 T variability, 30 to 34% for near-global-average T anomalies, with T increases associated with increases in aerosol loading. The latitudinal structure of regression coefficients (Figure 11) suggests significant warming during periods of large aerosol loading at all latitudes between 60°S and 45°N , with the largest response in the tropics, where both El Chichón and Mount Pinatubo are located, consistent with earlier observational analyses [e.g., Parker and Brownscombe, 1983; Angell, 1993; Robock, 2000; Free and Lanzante, 2009]. Previous studies [Driscoll et al., 2012; Thompson et al., 2012; Charlton-Perez et al., 2013] have suggested that many models simulate excessive warming following volcanic eruptions based on visual examination of simulated and observed T time series. A more quantitative evaluation could be made by comparing the magnitude of the T response to aerosols in these CDRs with that in global climate models and in chemistry-climate models.

Solar variability explains about 24% of the near-global-average T variability, and T increases are associated with increases in the 10.7 cm radio flux index. The response is significant between 45°S and 45°N and strongest at $\sim 25^\circ\text{N}$ and S latitudes. This result is qualitatively consistent with that of Randel et al. [2009b, Figure 27], although their regression analysis did not include ENSO or aerosol terms, the period of record was 4 years shorter, and the coefficients were expressed in different units. The ~ 0.15 K per standard deviation signal shown in Figure 11 corresponds to ~ 0.6 K change between solar maximum and minimum, which is about 50% larger than reported by Randel et al. [2009b]. Because aerosol variability has a time scale similar to that of the solar cycle during the period 1979–1995, and because the current solar cycle has been weaker than the

slope during 1995–2013, suggesting that a piecewise-linear function, with a breakpoint at January 1995, is a reasonable characterization of trend. This example is typical of results from the other CDRs in this study.

Tests of the sensitivity of regression coefficients to the date of the breakpoint revealed robust results; any breakpoint between July 1993 and July 1996 yields coefficients that fall well within the 95% confidence intervals of the coefficients obtained using January 1995 as a breakpoint. This is true for all predictors and for all near-global-average SSU and MSU CDRs. The following subsections report regression results using all of the predictors listed in section 2.2 and a trend breakpoint in January 1995.

3.2.2. Microwave Sounding Unit

Figure 10 (top) shows the percent variance explained by the regression predictors, and by the residuals, in near-global-average T anomalies, for all three MSU-4 CDRs. Because the QBO predictors each explain $<1\%$ of the variance in near-global averages, they

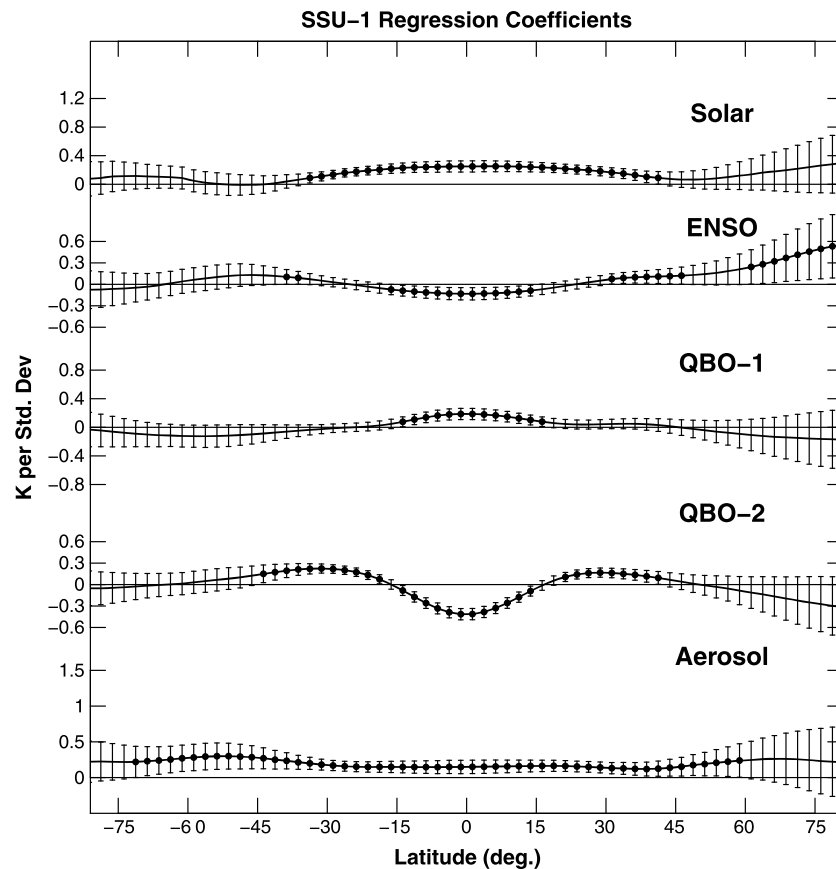


Figure 13. Regression coefficients (K per standard deviation) and their 95% confidence intervals as a function of latitude, at 2.5° latitude resolution, obtained from multiple linear regression of NOAA zonal-mean SSU-1 temperature anomaly time series. Coefficients are shown with filled circles at latitudes where the 95% confidence intervals do not encompass 0.

previous three, these regression coefficients are likely sensitive to the time period of the analysis. Indeed, analysis of the 19 year record 1995–2013 (not shown) suggested stronger solar signals than in the full record 1979–2013.

In the lower stratospheric region sampled by MSU-4, ENSO explains a larger fraction of global-mean T variability (13%) than does the QBO (<1%). Although regression coefficients for ENSO are not significantly different from 0 for near-global-average time series, the zonal results (Figure 11) indicate statistically significant signals, of opposite sign, in the tropics (15°N–15°S) and midlatitudes. The stratospheric T response to ENSO is cooling in the tropics and warming at higher latitudes during the El Niño phase. The tropical cooling has been attributed to enhanced tropical upwelling [Calvo *et al.*, 2010], and the high-latitude warming is consistent with the ENSO influence on the incidence of sudden stratospheric warmings [e.g., van Loon and Labitzke, 1987; Taguchi and Hartmann, 2006; Garfinkel and Hartmann, 2007]. Thus, while the global troposphere is known to warm in association with tropical tropospheric warming during El Niños [e.g., Seidel *et al.*, 2004], the latitude-dependent stratospheric T response, described by Randel *et al.* [2009a] and Free and Seidel [2009], does not strongly affect global-average stratospheric T . Similarly, although the two QBO predictors explain very little (<1%) global-average T variance, they are significant within narrow zonal bands, including both tropical and midlatitude regions, and are consistent among the three CDRs.

Because the MSU-4 weighting function extends below the tropical tropopause (typically found at ~16.5 km [Seidel *et al.*, 2001; Fu *et al.*, 2004], Figure 1), it is possible that the tropical regression coefficients underestimate the stratospheric response to ENSO, which is of opposite sign to the tropospheric response. Similarly, the deep vertical layer sampled by MSU-4 may mute the QBO signals, because the QBO does not extend into the upper troposphere.

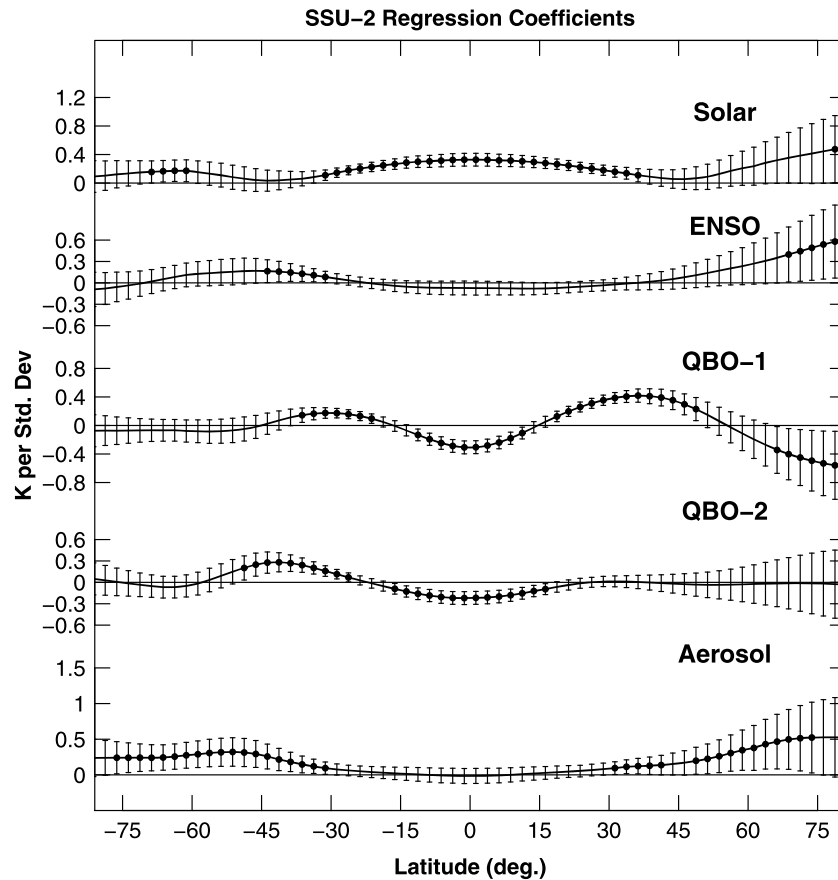


Figure 14. Same as Figure 13 but for SSU-2.

Trends are negative for both of the piecewise-linear segments in all three near-global-average MSU-4 CDRs, suggesting lower stratospheric cooling that is not explained by the other predictors, in particular aerosols. Near-global-average trends for the first segment (1979–1994) are ~ 0.4 K/decade and are highly significant, whereas trends for the second period (1995–2013) are ~ 0.05 K/decade and are not significantly different from 0.

The latitude dependence of the trends (Figure 12) indicates cooling at all latitudes during 1979–1994 (Figure 12, top), with smallest magnitudes (and not statistically significant in the UAH and RSS CDRs) in the deep tropics. In contrast, trends for 1995–2013 are statistically significant only in the tropics (Figure 12, bottom) and account for only $\sim 3\%$ of the total variance (Figure 10). Midlatitude cooling is smaller in magnitude, and the polar regions show warming trends that are not statistically significant.

The separation of the aerosol-related temperature changes from a simpler linear trend is noteworthy because previous studies [Pawson et al., 1998; Seidel and Lanzante, 2004] have speculated that the long-term cooling of the lower stratosphere seen in MSU-4 CDRs and in radiosonde data might be step-like in nature and associated with a “ratcheting down” of T after major volcanic eruptions. Instead, our regression analysis—and in particular the residual time series in Figure 9—suggests a more linear interpretation of the cooling. Both increases in atmospheric greenhouse gases and depletion of stratospheric ozone have long been identified as causes of potential [Manabe and Wetherald, 1967; Ramanathan et al., 1976] and observed [Shine et al., 2003; Ramaswamy et al., 2006; Gillett et al., 2011] long-term stratospheric cooling. If the changes in these atmospheric constituents dominate the trend estimates, then the differences between the strong cooling before 1995 and the insignificant trend thereafter suggests that ozone decreases dominate the anthropogenic signal in lower stratospheric temperatures, since total greenhouse gas concentrations have increased steadily over 1979–2013 whereas ozone depletion has slowed or reversed [IPCC, 2013; WMO, 2014]. Kyrölä et al. [2013], Bourassa et al. [2014] and Tummon et al. [2015] all show observational evidence for upper stratospheric ozone decreases before, and increases after, the late 1990s.

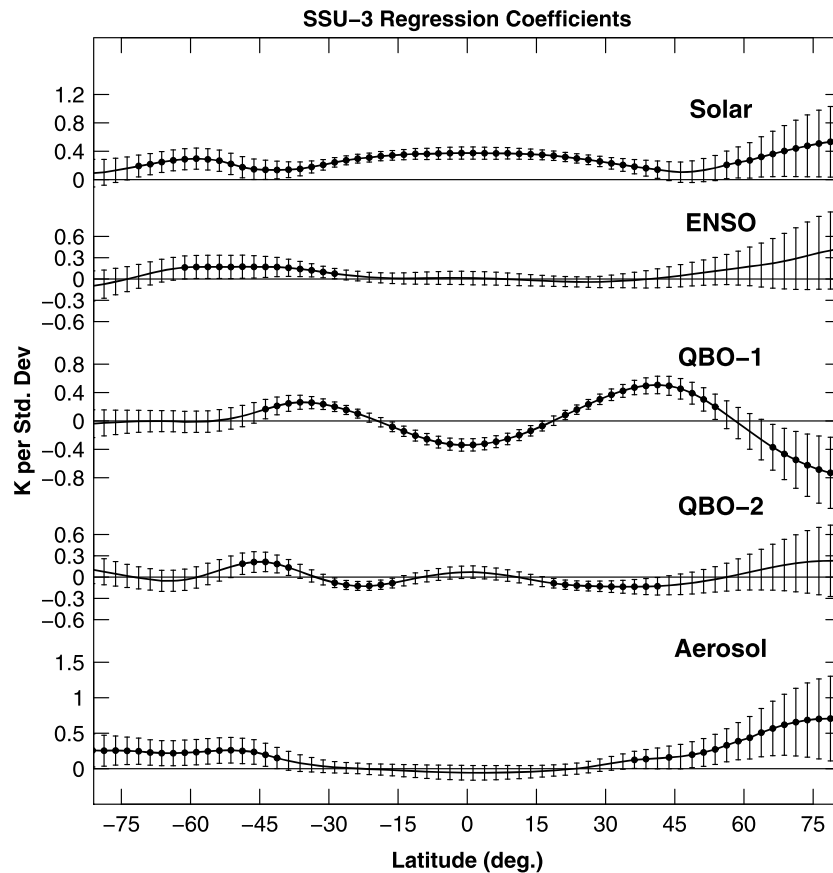


Figure 15. Same as Figure 13 but for SSU-3.

On the other hand, the latitudinal structure of 1979–1994 MSU-4 trends (Figure 12, top), with greater cooling near 30°N and S latitudes than in the tropics or midlatitudes, is consistent with the MSU-4 trends reported by *Fu et al.* [2006] and by *Fu and Lin* [2011], for 1979–2005 and 1979–2009, respectively. Those studies link the pattern of stratospheric cooling trends to poleward shifts in the jet streams. *Fu et al.* [2015] link the latitude dependence of observed 1980–2009 MSU-4 trends to changes in the Brewer-Dobson circulation, as predicted by climate models. Our 1995–2013 estimated MSU-4 trends (Figure 12, bottom) show no significant cooling at 30°N and S latitudes, suggesting that if circulation changes were a factor during 1979–1994, there may have been a reversal or weakening of those changes in later years.

3.2.3. Stratospheric Sounding Unit

We performed analogous regression analysis for both NOAA and UKMO near-global-average CDRs for the three SSU channels, which we summarize briefly before discussing the latitude-dependent results from the NOAA data. For all six near-global-average CDRs, the predictors explain about 90% of the *T* variance (Figure 10, bottom). The solar, ENSO, QBO, and aerosol regression coefficients (not shown) for the NOAA and UKMO CDRs agree within their respective confidence intervals for each SSU channel. This is not the case for trend estimates; except for SSU-1 trends for 1979–1994, the estimates derived from NOAA and UKMO CDRs do not have overlapping 95% confidence intervals. This lack of agreement remains despite the large magnitudes of the 1979–1994 trends (–0.5 to –1.4 K/decade), which explain the greatest fraction of variance (28 to 40%, Figure 10, bottom).

Figures 13–15 show regression coefficients as a function of latitude, the three SSU channels using NOAA CDRs spanning 1979–2005, and Figure 16 shows the zonal structure of the trend. Consistent with the near-global-average results, statistically significant cooling during 1979–1994 of ~–0.6 to –1.4 K/decade is evident at all latitudes outside the polar zone for all three channels. In contrast, trend estimates for 1995–2005 (not shown) are not statistically significant at any latitude.

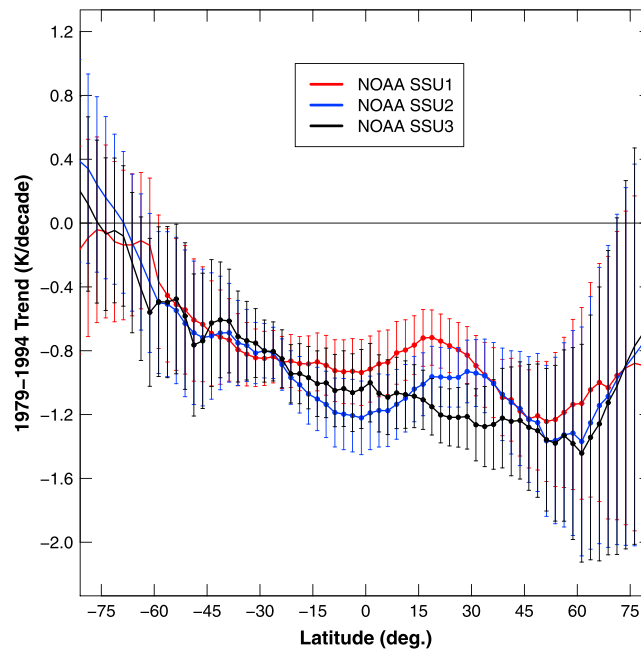


Figure 16. Estimates of 1979–1994 trends (K per decade), as a function of latitude, and their 95% confidence intervals, obtained from multiple linear regression of zonal-mean SSU-1, SSU-2, and SSU-3 temperature anomaly time series. Estimates are shown as filled circles at latitudes where the 95% confidence intervals do not encompass 0.

ing altitude in the stratosphere (Figure 10). The aerosol signal is statistically significant at all nonpolar latitudes for SSU-1, but for SSU-2 and SSU-3 the signal is not significant in the tropics and is strongest at high latitudes (Figures 13–15). The decrease of the aerosol signal from the lower to the upper stratosphere is consistent with results based on reanalysis data [e.g., Simmons *et al.*, 2014].

ENSO variability explains 5–10% of the variability in SSU CDRs (Figure 10), and the zonal coefficients show tropical and extratropical responses, of opposite sign, in SSU-1 (Figure 13), with the extratropical signals also evident in SSU-2 and SSU-3 (Figures 14 and 15). The pattern of tropical-extratropical connections seen in both the aerosol and ENSO coefficients is likely due to stratospheric dynamical responses to changes initiated in the tropical lower stratosphere. In the aerosol case, the T response could be either purely dynamical or could involve a radiative response to aerosols transported from their tropical source region to higher latitudes.

The two QBO terms together explain $< 1\%$ of the variance in any of the near-global-average SSU CDRs. Nevertheless, the zonal coefficients reveal both the downward propagating equatorial QBO signal and responses at higher latitudes. The two orthogonal QBO predictor time series (Figure 2) have ~ 8 month lag (with QBO-1 leading QBO-2) to capture the downward propagation of equatorial stratospheric zonal wind reversals. Regression coefficients for QBO-1 are significant and negative near the equator for SSU-3 (Figure 15), which samples the upper stratosphere, positive for SSU-1 in the lower stratosphere (Figure 13), and not significant for MSU-4 (not shown), whose weighting function includes the tropical lower stratosphere and upper troposphere. The QBO-2 coefficients in the tropics show a reversed pattern, with SSU-3 (Figure 15) showing no significant response but SSU-2, SSU-1, and MSU-4 showing tropical responses of opposite sign to their QBO-1 responses. Oppositely signed midlatitude coefficients suggest stratospheric QBO-related circulation cells outside the tropics [Holton and Tan, 1980; Baldwin *et al.*, 2001]. These patterns may be useful in evaluating climate model simulations of the QBO, which has recently been successfully reproduced in some models [Charlton-Perez *et al.*, 2013].

4. Conclusions

This study sought to build upon earlier analyses of observed stratospheric T change by examining new and extended versions of satellite CDRs and by using multiple regression analysis to identify major patterns of T

The second most important predictor, explaining 17 to 25% of the variance in the near-global-average data (Figure 10), is solar variability. The zonal structures of the solar signals, based on the NOAA CDRs (Figures 13–15), are in good agreement with the structure described by Randel *et al.* [2009b], based on an earlier version of UKMO data (which was only available in zonal bands). In both analyses, the strongest solar signals are in the tropics, their strength increases with increasing altitude, and they are not statistically significant in the extratropics for SSU-1 or SSU-2. The magnitudes of the signals are also in good accord, which is somewhat surprising in light of the differences in the approaches to the regression analyses and the CDR differences.

Variations in stratospheric aerosol loading, the most important predictor for MSU-4 T changes, is the third-ranking predictor for all three SSU channels, explaining decreasing percentages of variance with increas-

variability. The main distinctions of this study are the use of new SSU CDRs; the use of longer, and in some cases more spatially resolved, CDRs; inclusion of six different predictors in regression analyses; and treatment of trends as piecewise-linear functions.

Despite recent efforts to improve and extend various CDRs, there remain observational gaps that could be filled to further advance understanding of stratospheric T changes during the satellite era. Currently, CDRs for SSU and AMSU end in 2005 and 2011, respectively. Key needs for stratospheric T CDRs are extension of AMSU CDRs for the six AMSU stratospheric channels to cover 1999 to the present and a merging of gridded SSU and AMSU records for the three SSU channels to cover 1979 to the present.

Such CDRs are uniquely valuable as T records derived from observations. They are derived from and complement fundamental climate data records (FCDRs, i.e., reprocessed satellite observed radiances), which are closer to the observed brightness temperatures but farther from atmospheric T . Reanalyses assimilate the FCDR radiances from atmospheric sounders and other data to estimate T fields that can be used in studies of long-term variability and trend [Simmons *et al.*, 2014]. Continued preservation and homogenization of the FCDRs from all sensors for inclusion in atmospheric reanalysis should improve the quality of reanalysis T fields.

Our main findings, which relate to T anomalies from which the mean annual cycle have been removed, are as follows:

1. Differences remain among the MSU-4 CDRs from three research teams. The RSS and NOAA CDRs are highly correlated everywhere, but their near-global-average T anomaly time series have a time-varying bias of ~ 0.1 K over the period 1979–2013, during which time monthly T anomalies had ~ 2 K range and indicate long-term cooling. The UAH CDR shows larger differences from the other two, with lower correlations in regions outside the tropical belt, and a time-varying bias of ~ 0.2 K indicating more pronounced cooling. These differences are related to a previously unreported inhomogeneity in version 5 of the UAH CDR, which exhibits a large increase in the spatial variability of T anomalies in 2005. A newly released test version 6 of UAH data does not exhibit this feature.
2. The two most recent versions of SSU CDRs offer limited opportunity for comparison, because the UKMO CDR is available only as global-average data at 6 month resolution. Since the study by Thompson *et al.* [2012], both NOAA and UKMO SSU CDRs have been reprocessed and documented [Zou *et al.*, 2014; Nash and Saunders, 2015], and differences between them have been reduced but not eliminated. For all three SSU channels, the two CDRs differ by up to ± 0.5 K. Cooling over 1979–2005 is seen in all CDRs, with the NOAA record showing more cooling than UKMO for SSU-1 and SSU-3 and less cooling than UKMO for SSU-2.
3. Multiple regression analysis reveals solar, ENSO, QBO, aerosol, and piecewise-linear trend signals in the CDRs, and these predictors combine to explain ~ 80 to 90% of the variance in global anomaly time series. The most important predictor variables (in terms of the percent variance in near-global-average T explained) are aerosols, solar variability, and ENSO for MSU-4 and linear trends for all three SSU channels.
4. Estimates of T trends, separated from T changes associated with other predictors in the regression analyses, are well described by piecewise-linear changes with a breakpoint at January 1995. Highly significant cooling during 1979–1994 is followed by periods (ending in 2005 for SSU and in 2013 for MSU-4) in which trends, on global average, are not significantly different from 0. More recent AMSU CDRs suggest a continuing lack of trend in the lower stratosphere but cooling at higher altitudes during 1999–2011.
5. Regression coefficients and trends have distinct latitude dependence. In some cases (such as ENSO and QBO), predictors that explain very little variance in global-average T are highly significant in particular latitude bands.

These results, and the CDRs on which they are based, may be useful in evaluating global climate model and chemistry-climate model simulations of past stratospheric T variations. Such models should be able to reproduce both the near-global-average variations and the latitudinal patterns of change associated with different explanatory variables. Some previous model intercomparison studies have lacked observational results against which to compare model simulations [e.g., Austin *et al.*, 2008], used versions of CDRs that have now been revised [e.g., Shine *et al.*, 2003; Gillett *et al.*, 2011], or relied on reanalyses that assimilated unadjusted stratospheric T observations [e.g., Butchart *et al.*, 2011]. The findings of these studies could be reevaluated using CDR-based observational results.

Future work could also address the lack of global-mean lower stratospheric T trends since 1995 using longer and different observational data records and using mechanistic models to investigate the roles of different processes.

Extensions of the CDRs used here, as mentioned above, as well as CDRs derived from more recent observing systems, such as Global Navigational Satellite System Radio Occultation data [e.g., Steiner *et al.*, 2013], NASA Microwave Limb Sounder [Schwartz *et al.*, 2008], NASA Sounding of the Atmosphere using Broadband Emission Radiometry data (Randel *et al.*, in preparation), and European Space Agency Michelson Interferometer for Passive Atmospheric Sounding data [García-Comas *et al.*, 2014], could be usefully exploited in such investigations.

Acknowledgments

The authors thank Praveena Krishnan (NOAA), Qiang Fu (University of Washington), and Adrian Simmons (ECMWF) for helpful reviews of the manuscript. All data sets used in this analysis are publically available as described in section 2. The views, opinions, and findings in this report are those of the authors and should not be construed as official National Oceanic and Atmospheric Administration or U.S. Government position, policy, or decision.

References

- Angell, J. K. (1993), Comparison of stratospheric warming following Agung, El Chichon and Pinatubo volcanic eruptions, *Geophys. Res. Lett.*, *20*, 715–718.
- Austin, J., *et al.* (2008), Coupled chemistry climate model simulations of the solar cycle in ozone and temperature, *J. Geophys. Res.*, *113*, D11306, doi:10.1029/2007JD009391.
- Baldwin, M. P., *et al.* (2001), The quasi-biennial oscillation, *Rev. Geophys.*, *39*(2), 179–229, doi:10.1029/1999RG000073.
- Bourassa, A. E., D. A. Degenstein, W. J. Randel, J. M. Zawodny, E. Kyrölä, C. A. McLinden, C. E. Sioris, and C. Z. Roth (2014), Trends in stratospheric ozone derived from merged SAGE II and Odin-OSIRIS satellite observations, *Atmos. Chem. Phys.*, *14*, 6983–6994, doi:10.5194/acp-14-6983-2014.
- Butchart, N., *et al.* (2011), Multimodel climate and variability of the stratosphere, *J. Geophys. Res.*, *116*, D05102, doi:10.1029/2010JD014995.
- Calvo Fernandez, N., R. R. Garcia, R. G. Herrera, D. G. Puyol, L. G. Presa, E. H. Martin, and P. R. Rodriguez (2004), Analysis of the ENSO signal in tropospheric and stratospheric temperatures observed by MSU, 1979–2000, *J. Clim.*, *17*, 3934–3946.
- Calvo, N., R. R. Garcia, W. J. Randel, and D. Marsh (2010), Dynamical mechanism for the increase in tropical upwelling in the lowermost tropical stratosphere during warm ENSO events, *J. Atmos. Sci.*, *67*, 2331–2340.
- Charlton-Perez, A., *et al.* (2013), On the lack of stratospheric dynamical variability in low-top versions of the CMIP5 models, *J. Geophys. Res.*, *118*, 2494–2505, doi:10.1002/jgrd.50125.
- Christy, J. R., R. W. Spencer, W. B. Norris, and W. D. Braswell (2003), Error estimates of version 5.0 of MSU-AMSU bulk atmospheric temperature, *J. Atmos. Oceanic Technol.*, *20*, 613–629.
- Dee, D. P., E. Källén, A. J. Simmons, and L. Haimberger (2010), Comments on “Reanalyses suitable for characterizing longterm trends”, *Bull. Am. Meteorol. Soc.*, *92*, 65–70, doi:10.1175/2010BAMS3070.1.
- Driscoll, S., A. Bozzo, L. J. Gray, A. Robock, and G. Stenchikov (2012), Coupled Model Intercomparison Project 5 (CMIP5) simulations of climate following volcanic eruptions, *J. Geophys. Res.*, *117*, D17105, doi:10.1029/2012JD017607.
- Errera, Q., M. Fujiwara, C. Long, and D. Jackson (2015), Report from the 10th SPARC data assimilation workshop and the 2014 SPARC Reanalysis Intercomparison Project (S-RIP) workshop in Washington DC, USA. SPARC Newsletter, No. 44, 31–38, January 2015. [Available at http://www.sparc-climate.org/fileadmin/customer/6_Publications/Newsletter_PDF/44_SPARCnewsletter_Jan2015_WEB.pdf]
- Ferraro, A. J., M. Collins, and F. H. Lambert (2015), A hiatus in the stratosphere, *Nat. Clim. Change*, *5*, 497–498, doi:10.1038/nclimate2624.
- Forbes, J. M., X. Zhang, and D. R. Marsh (2014), Solar cycle dependence of middle atmosphere temperatures, *J. Geophys. Res. Atmos.*, *119*, 9615–9625, doi:10.1002/2014JD021484.
- Free, M., and D. J. Seidel (2009), Observed El Niño–Southern Oscillation temperature signal in the stratosphere, *J. Geophys. Res.*, *114*, D23108, doi:10.1029/2009JD012420.
- Free, M., and J. R. Lanzante (2009), Effect of volcanic eruptions on the vertical temperature profile in radiosonde data and climate models, *J. Clim.*, *22*, 2925–2939, doi:10.1175/2008JCLI2562.1.
- Fu, Q., and P. Lin (2011), Poleward shift of subtropical jets inferred from satellite-observed lower stratospheric temperatures, *J. Clim.*, *24*, 5597–5603, doi:10.1175/JCLI-D-11-00027.1.
- Fu, Q., C. M. Johanson, S. G. Warren, and D. J. Seidel (2004), Contribution of stratospheric cooling to satellite-inferred tropospheric temperature trends, *Nature*, *429*, 55–58, doi:10.1038/nature02524.
- Fu, Q., C. M. Johanson, J. M. Wallace, and T. Reichler (2006), Enhanced mid-latitude tropospheric warming in satellite measurements, *Science*, *312*, 1179.
- Fu, Q., P. Lin, S. Solomon, and D. L. Hartmann (2015), Observational evidence of strengthening of the Brewer-Dobson circulation since 1980, *J. Geophys. Res. Atmos.*, *120*, 10,214–10,228, doi:10.1002/2015JD023657.
- García-Comas, M., *et al.* (2014), MIPAS temperature from the stratosphere to the lower thermosphere: Comparison of vM21 with ACE-FTS, MLS, OSIRIS, SABER, SOFIE and lidar measurements, *Atmos. Meas. Tech.*, *7*, 3633–3651, doi:10.5194/amt-7-3633-2014.
- Garfinkel, C. I., and D. L. Hartmann (2007), The effects of the Quasi-Biennial Oscillation and the El-Niño Southern Oscillation on polar temperatures in the stratosphere, *J. Geophys. Res.*, *112*, doi:10.1029/2007JD008481.
- Gillett, N. P., *et al.* (2011), Attribution of observed changes in stratospheric ozone and temperature, *Atmos. Chem. Phys.*, *11*, 599–609.
- Holton, J. R., and H.-C. Tan (1980), The influence of the equatorial quasi-biennial oscillation on the global circulation at 50 mb, *J. Atmos. Sci.*, *37*, 2200–2208.
- Hood, L. L., B. E. Soukharev, and J. P. McCormack (2010), Decadal variability of the tropical stratosphere: Secondary influence of the El Niño–Southern Oscillation, *J. Geophys. Res.*, *115*, D11113, doi:10.1029/2009JD012291.
- IPCC (2013), Summary for policymakers, in *Climate Change 2013: The Physical Science Basis. Contribution of Working Group I to the Fifth Assessment Report of the Intergovernmental Panel on Climate Change*, edited by T. F. Stocker *et al.*, Cambridge Univ. Press, Cambridge, U. K., and New York.
- Kobayashi, S., *et al.* (2015), The JRA-55 reanalysis: General specifications and basic characteristics, *J. Meteorol. Soc. Jpn.*, *93*(1), 5–48, doi:10.2151/jmsj.2015-001.
- Kyrölä, E., M. Laine, V. Sofieva, J. Tamminen, S.-M. Päiväranta, S. Tukiainen, J. Zawodny, and L. Thomason (2013), Combined SAGE II-GOMOS ozone profile data set for 1984–2011 and trend analysis of the vertical distribution of ozone, *Atmos. Chem. Phys.*, *13*, 10,645–10,658, doi:10.5194/acp-13-10645-2013.
- Long, C. S., and J. R. Christy (2014), [Temperature] Lower stratospheric temperature [in “State of the Climate in 2013”], *Bull. Am. Meteorol. Soc.*, *95*, S14–S15.
- Manabe, S., and R. Wetherald (1967), Thermal equilibrium of the atmosphere with a given distribution of relative humidity, *J. Atmos. Sci.*, *24*, 241–259.

- McLandsress, C., T. G. Shepherd, A. I. Jonsson, T. von Clarmann, and B. Funke (2015), A method for merging nadir-sounding climate records, with an application to the global-mean stratospheric temperature data sets from SSU and AMSU, *Atmos. Chem. Phys. Discuss.*, *15*, 10,085–10,122, doi:10.5194/acpd-15-10085-2015.
- Mears, C. A., and F. J. Wentz (2009), Construction of the Remote Sensing Systems V3.2 atmospheric temperature records from the MSU and AMSU microwave sounders, *J. Atmos. Oceanic Technol.*, *26*, 1040–1056.
- Mears, C. A., F. J. Wentz, P. Thorne, and D. Bernie (2011), Assessing uncertainty in estimates of atmospheric temperature changes from MSU and AMSU using a Monte-Carlo estimation technique, *J. Geophys. Res.*, *116*, D08112, doi:10.1029/2010JD014954.
- Mitchell, D. M., et al. (2014), Signatures of naturally induced variability in the atmosphere using multiple reanalysis datasets, *Q. J. R. Meteorol. Soc.*, doi:10.1002/qj.2492.
- Nash, J., and R. Saunders (2015), A review of Stratospheric Sounding Unit radiance observations for climate trends and reanalyses, *Q. J. R. Meteorol. Soc.*, *141*, 2103–2113, doi:10.1002/qj.2505.
- Naujokat, B. (1981), Long-term variations in the stratosphere of the Northern Hemisphere during the last two sunspot cycles, *J. Geophys. Res.*, *86*, 9811–9816.
- Naujokat, B. (1986), An update of the observed quasi-biennial oscillation of the stratospheric winds over the tropics, *J. Atmos. Sci.*, *43*, 1873–1877.
- Parker, D. E., and J. K. L. Brownscombe (1983), Stratospheric warming following the El Chichón volcanic eruption, *Nature*, *301*, 406–408.
- Pawson, S., K. Labitzke, and S. Leder (1998), Stepwise changes in stratospheric temperature, *Geophys. Res. Lett.*, *25*, 2157–2160.
- Ramanathan, V., L. B. Callis, and R. E. Boughner (1976), Sensitivity of surface-temperature and atmospheric-temperature to perturbations in stratospheric concentration of ozone and nitrogen-dioxide, *J. Atmos. Sci.*, *33*, 1092–1112.
- Ramaswamy, V., et al. (2001), Stratospheric temperature trends: Observations and model simulations, *Rev. Geophys.*, *39*, 71–122.
- Ramaswamy, V., M. D. Schwarzkopf, W. J. Randel, B. D. Santer, B. J. Soden, and G. Stenchikov (2006), Anthropogenic and natural influences in the evolution of lower stratospheric cooling, *Science*, *311*, doi:10.1126/science.1122587.
- Randel, W. J., F. Wu, R. Swinbank, J. Nash, and A. O'Neill (1999), Global QBO circulation derived from UKMO stratospheric analyses, *J. Atmos. Sci.*, *56*, 457–474.
- Randel, W. J., R. R. Garcia, N. Calvo, and D. Marsh (2009a), ENSO influence on zonal mean temperature and ozone in the tropical lower stratosphere, *Geophys. Res. Lett.*, *36*, L15822, doi:10.1029/2009GL039343.
- Randel, W. J., et al. (2009b), An update of observed stratospheric temperature trends, *J. Geophys. Res.*, *114*, D02107, doi:10.1029/2008JD010421.
- Robock, A. (2000), Volcanic eruptions and climate, *Rev. Geophys.*, *38*, 191–219.
- Sato, M., J. E. Hansen, M. P. McCormick, and J. B. Pollack (1993), Stratospheric aerosol optical depth, 1850–1990, *J. Geophys. Res.*, *98*, 22,987–22,994.
- Schwartz, M. J., et al. (2008), Validation of the aura microwave limb sounder temperature and geopotential height measurements, *J. Geophys. Res.*, *113*, D15511, doi:10.1029/2007JD008783.
- Seidel, D. J., and J. R. Lanzante (2004), An assessment of three alternatives to linear trends for characterizing global atmospheric temperature changes, *J. Geophys. Res.*, *109*, D14108, doi:10.1029/2003JD004414.
- Seidel, D. J., R. J. Ross, J. K. Angell, and G. C. Reid (2001), Climatological characteristics of the tropical tropopause as revealed by radiosondes, *J. Geophys. Res.*, *106*, 7857–7878, doi:10.1029/2000JD900837.
- Seidel, D. J., et al. (2004), Uncertainty in signals of large-scale climate variations in radiosonde and satellite upper-air temperature datasets, *J. Clim.*, *17*, 2225–2240.
- Seidel, D. J., N. P. Gillett, J. R. Lanzante, K. P. Shine, and P. W. Thorne (2011), Stratospheric temperature trends: Our evolving understanding, *Wiley Interdiscip. Rev. Clim. Change*, *2*, 592–616, doi:10.1002/wcc.125.
- Shine, K. P., et al. (2003), A comparison of model-predicted trends in stratospheric temperatures, *Q. J. R. Meteorol. Soc.*, *129*, 1565–1588, doi:10.1256/qj.02.186.
- Simmons, A. J., P. Poli, D. P. Dee, P. Berrisford, H. Hersbach, S. Kobayashi, and C. Peubey (2014), Estimating low-frequency variability and trends in atmospheric temperature using ERA-Interim, *Q. J. R. Meteorol. Soc.*, *140*, 329–353, doi:10.1002/qj.2317.
- Steiner, A. K., et al. (2013), Quantification of structural uncertainty in climate data records from GPS radio occultation, *Atmos. Chem. Phys.*, *13*, 1469–1484, doi:10.5194/acp-13-1469-2013.
- Taguchi, M., and D. L. Hartmann (2006), Increased occurrence of stratospheric sudden warmings during El Niño as simulated WACCM, *J. Clim.*, *19*, 324–332.
- Tapping, K. F., and D. C. Morton (2013), The next generation of Canadian solar flux monitoring, *J. Phys. Conf. Ser.*, *440*, 012039, doi:10.1088/1742-6596/440/1/012039.
- Thompson, D. W. J., and S. Solomon (2009), Understanding recent stratospheric climate change, *J. Clim.*, *22*, 1934–1943.
- Thompson, D. W. J., D. J. Seidel, W. J. Randel, C.-Z. Zou, A. H. Butler, R. Lin, C. Long, C. Mears, and A. Osso (2012), The mystery of recent stratospheric temperature trends, *Nature*, *491*, 692–697, doi:10.1038/nature11579.
- Thorne, P. W., and R. S. Vose (2010), Reanalyses suitable for characterizing long-term trends: Are they really achievable?, *Bull. Am. Meteorol. Soc.*, *91*, 353–361.
- Thorne, P. W., D. E. Parker, J. R. Christy, and C. A. Mears (2005), Uncertainties in climate trends: Lessons from upper-air temperature records, *Bull. Am. Meteorol. Soc.*, *86*, 1437–1442, doi:10.1175/BAMS-86-10-1437.
- Tummon, F., et al. (2015), Intercomparison of vertically resolved merged satellite ozone data sets: Interannual variability and long-term trends, *Atmos. Chem. Phys.*, *15*, 3021–3043, doi:10.5194/acp-15-3021-2015.
- van Loon, H., and K. Labitzke (1987), The Southern Oscillation. Part V: The anomalies in the lower stratosphere of the Northern Hemisphere in winter and a comparison with the quasi-biennial oscillation, *Mon. Weather Rev.*, *115*, 357–369.
- Wallace, J. M., L. Panetta, and J. Estberg (1993), A phase-space representation of the equatorial stratospheric quasi-biennial oscillation, *J. Atmos. Sci.*, *50*, 1751–1762.
- Wang, W., and C.-Z. Zou (2014), AMSU-A-only atmospheric temperature data records from the lower troposphere to the top of the stratosphere, *J. Atmos. Oceanic Technol.*, *31*, 808–825, doi:10.1175/JTECH-D-13-00134.1.
- WMO (World Meteorological Organization) (2014), Assessment for decision-makers: Scientific assessment of ozone depletion: 2014, Global Ozone Research and Monitoring Project—Report No. 56, Geneva, Switzerland, 88 pp.
- Wolter, K., and M. S. Timlin (2011), El Niño/Southern Oscillation behaviour since 1871 as diagnosed in an extended multivariate ENSO index (MEI.ext), *Int. J. Climatol.*, *31*, 1074–1087, doi:10.1002/joc.2336.
- Zou, C.-Z., M. Goldberg, Z. Cheng, N. Grody, J. Sullivan, C. Cao, and D. Tarpley (2006), Recalibration of microwave sounding unit for climate studies using simultaneous nadir overpasses, *J. Geophys. Res.*, *111*, D19114, doi:10.1029/2005JD006798.
- Zou, C.-Z., H. Qian, W. Wang, L. Wang, and C. Long (2014), Recalibration and merging of SSU observations for stratospheric temperature trend studies, *J. Geophys. Res. Atmos.*, *119*, 13,180–13,205, doi:10.1002/2014JD021603.